

Chapter 6

Study of Breakup Effect of Weakly Bound Projectile around Coulomb Barrier Energies for ${}^6\text{Li}+{}^{100}\text{Mo}$ System

6.1 Introduction

Weakly bounded heavy ions study of reaction dynamics has played a very curious role for several decades specifically around the barrier energies of the system, both experimentally and theoretically [1, 2, 3, 4]. The development of theoretical techniques and their dependence on experimental data for executing the coupled reaction channel calculations has contributed to the advancement of our understanding of the way the structure of an incoming nucleus impacts the reaction dynamics. The channel coupling effects specifically pronounce at energies nearby Coulomb barrier. This may be understood audibly in context of improving near-barrier and sub-

Chapter 6: *Study of Breakup Effect of Weakly Bound Projectile around Coulomb Barrier Energies for ${}^6\text{Li}+{}^{100}\text{Mo}$ System*

barrier fusion as well as through the breakup threshold anomaly, an abnormality at a threshold. [5]. Special attention to loosely bound nuclei can be possibly implemented because of rich technical abundance of radioactive ion beams (RIBs). With use of RIB and WBP, it is possible to get valuable insight into the included degrees of freedom of nuclei by studying the numerous channels surrounding the barrier, including transfer, breakup, and fusion as well as elastic and inelastic scattering. A useful tool for understanding the kinetics of nuclear reaction is the analysis of the optical potential behaviour that arises in elastic scattering under the influence of any of the aforementioned absorption channels. From the systematic analysis, a "Threshold Anomaly (TA)" surrounds the barrier in the energy dependence of the phenomenological optical potential for strong bound systems. However, in the dynamics of WBP, TA is not noticed. Under these circumstances, breakup cross section appears to be rather considerable even below the Coulomb barrier, which raises the imaginary potential. This increment may be consistent as bombarding energy decreases. Real part of potential declines with its rising imaginary portion. This energy-dependent behaviour is a result of causality and is included in the dispersion relation, which connects the real and imaginary components of potential. [5]. This atypical dependence is Breakup Threshold Anomaly (BTA). A systematic and predictable theoretical development requires a huge collection of experimental data with all the possible collection of combinations of projectiles and targets [6, 7]. In this work, we have incorporated an elastic scattering study of WBP ${}^6\text{Li}$ with a middle mass target ${}^{100}\text{Mo}$ [8].

6.2 Experimental setup

The present work was carried out at General Purpose Scattering Chamber (GPSC) with 15 UD Pelletron accelerator at Inter University Accelerator Centre (IUAC). The measurement was done using a ${}^6\text{Li}^{3+}$ ion beam at incident energies 28, 25, 23, 21.5, 19, 17.5 and 15 MeV at beam current between 5-28 nA. A carbon backed ${}^{100}\text{Mo}$ (99.05% enriched) target was used of thickness 305 $\mu\text{g}/\text{cm}^2$ with carbon backing of $\sim 22\mu\text{g}/\text{cm}^2$. At the IUAC target laboratory, the targets were made using an e-gun technology for physical vapour deposition under a very high vacuum [9]. Seven silicon surface barrier detectors with $\Delta E+E$ telescope as detector setup covering 15° to 168° angular range. Figure 6.1 shows the experimental arrangement of detectors and other components and the internal view of the experimental arrangement of the chamber. For beam monitoring and absolute normalization two surface barrier monitor detectors with a thickness of 300 μm at $\pm 10^\circ$. The detectors thickness were, T1 having $\Delta E=40\mu\text{m}$ and $E=2$ mm, T2 with $\Delta E=40\mu\text{m}$ and $E=1$ mm, T3, T4, T5 detectors possessing $\Delta E=25\mu\text{m}$ and $E=1$ mm, T6 and T7 with $\Delta E=25\mu\text{m}$ and $E=300$ μm . T1-T5 detectors were kept at a rotating arm with 6° separation between each and T6 and T7 were fixed at back angles 156° and 168° . Each detector is collimated and thus covers an angle between 0.9 msr to 6 msr. The data were recorded using the software FREEDOM [10] and analyzed using the Linux-based data acquisition system LAMPS [11].

for ${}^6\text{Li}+{}^{100}\text{Mo}$ System

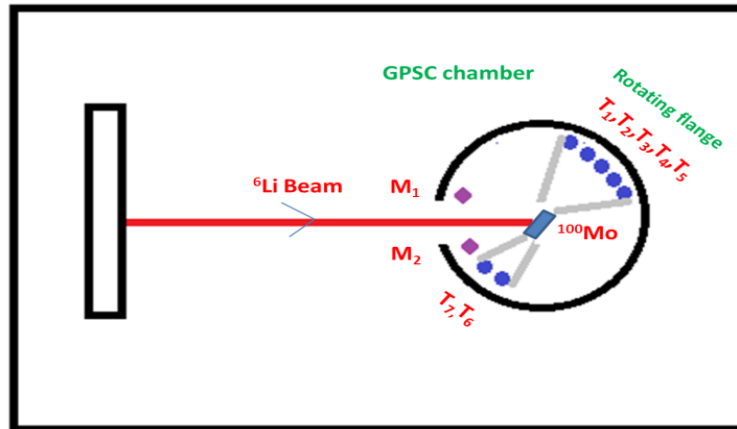


Figure 6.1: *Schematic diagram and inner view of GPSC chamber of the experimental setup for the experiment.*

6.3 Experimental and Theoretical Analysis

Woods-Saxon potential (WSP) was used to analyze the angular distribution of elastic scattering. Phenomenological fits are employed to determine Radius of Sensitivity and this information is utilized to establish the energy dependence of potential parameters.

6.3.1 Optical Model Analysis

6.3.1.1 Wood-Saxon Potential (WSP) model analysis

The total potential is given as the sum of Coulomb and nuclear potential as follows-

$$V(r, E) = V_C(r) + \frac{-V_0}{1 + \exp(r - R_V)/a_V} + i \frac{-W_0}{1 + \exp(r - R_W)/a_W} \quad (1)$$

Here, $V_C(r)$ is Coulomb potential, $R_V = r_v (A_P^{(1/3)} + A_T^{(1/3)})$ and $R_W = r_w (A_P^{(1/3)} + A_T^{(1/3)})$, A_P and A_T are masses of projectile and target respectively. The depths of potential for both components (V_0 , W_0), geometrical parameters (r_v , r_w), and diffuseness parameters (a_v , a_w) were all altered in simultaneously to find the parameters that best suit the experimental results. The Akyüz-Winther potential served as the source for the initial depth parameters for fitting. [12]. SFRESCO was used for elastic scattering data analysis with FRESCO code, version FRES 3.1 [13].

Chapter 6: *Study of Breakup Effect of Weakly Bound Projectile around Coulomb Barrier Energies for ${}^6\text{Li}+{}^{100}\text{Mo}$ System*

The search for parameters was within χ^2/N range $\chi^2 = \chi^2_{\min} + \chi^2_{\min}/2$. The errors obtained in reaction cross sections and fittings are decided by acceptable ranges. The obtained best fitted values are given in tables 6.1 and the angular distribution is plotted in figure 6.2 in black solid lines. The fitting procedure is further used to estimate the radius of sensitivity for real and imaginary potential. The finding procedure includes a variation of diffuseness parameter in the difference of some fixed steps nearby the best fit values to obtain a family of curves satisfying potential parameters. The crossing point of these curves gives the radius of sensitivity. An average sensitivity radius was found ~ 10.97 fm for ${}^6\text{Li}+{}^{100}\text{Mo}$ system. The corresponding plot of the sensitivity radius for ${}^6\text{Li}+{}^{100}\text{Mo}$ system is given in figure 6.3 (a) and (b) for the real part at energy 23. Using the dispersion relation, the energy dependence of potential parameters is determined at this sensitivity radius [14, 15].

for ${}^6\text{Li}+{}^{100}\text{Mo}$ System

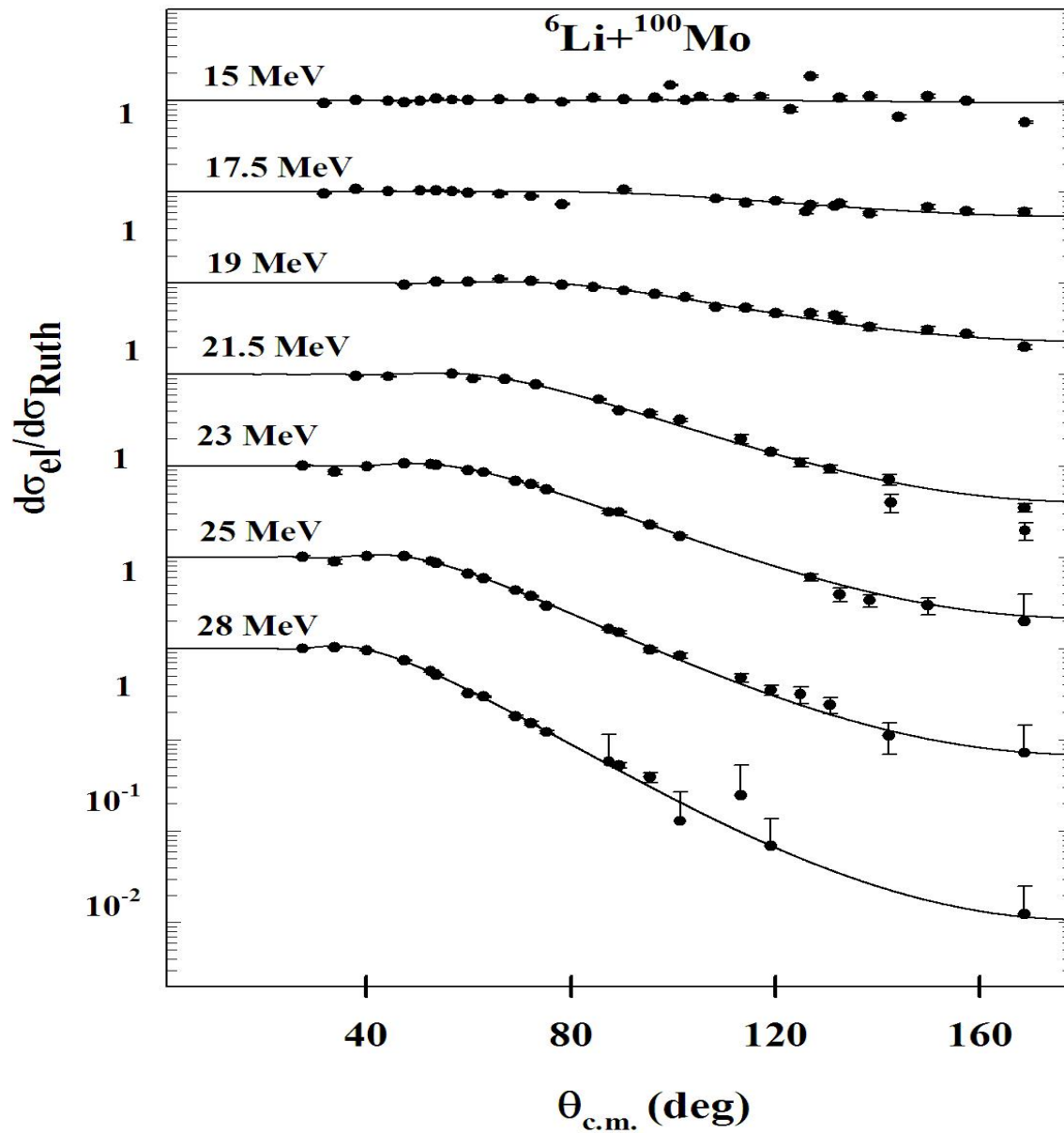


Figure 6.2: Elastic scattering angular distribution data fitting through Woods –Saxon potential

(solid line). Circles are experimental data points for system ${}^7\text{Li}+{}^{100}\text{Mo}$.

Table 6.1

Best fit optical potential parameters from SFRESCO of elastic scattering data and N represents the number of data points for the system ${}^6\text{Li}+{}^{100}\text{Mo}$.

E (MeV)	V (MeV)	Rv (fm)	av (fm)	W (MeV)	rv (fm)	av (fm)	χ^2	CS (mb)
27.95	32.7	1.24	0.51	32.4	1.11	0.84	6.29	1375
24.94	33.9	1.24	0.52	25.0	1.1	0.86	4.15	1057
22.39	42.0	1.24	0.58	33.3	1.18	0.73	2.11	871
21.44	61.4	1.24	0.50	33.8	1.13	0.79	8.53	755
18.93	25.0	1.24	0.69	69.9	1.25	0.54	3.12	365
17.43	72.0	1.24	0.47	68.7	1.23	0.59	10.6	182
14.92	25.5	1.24	0.79	30.0	1.1	0.48	1.2	1.84

for ${}^6\text{Li}+{}^{100}\text{Mo}$ System

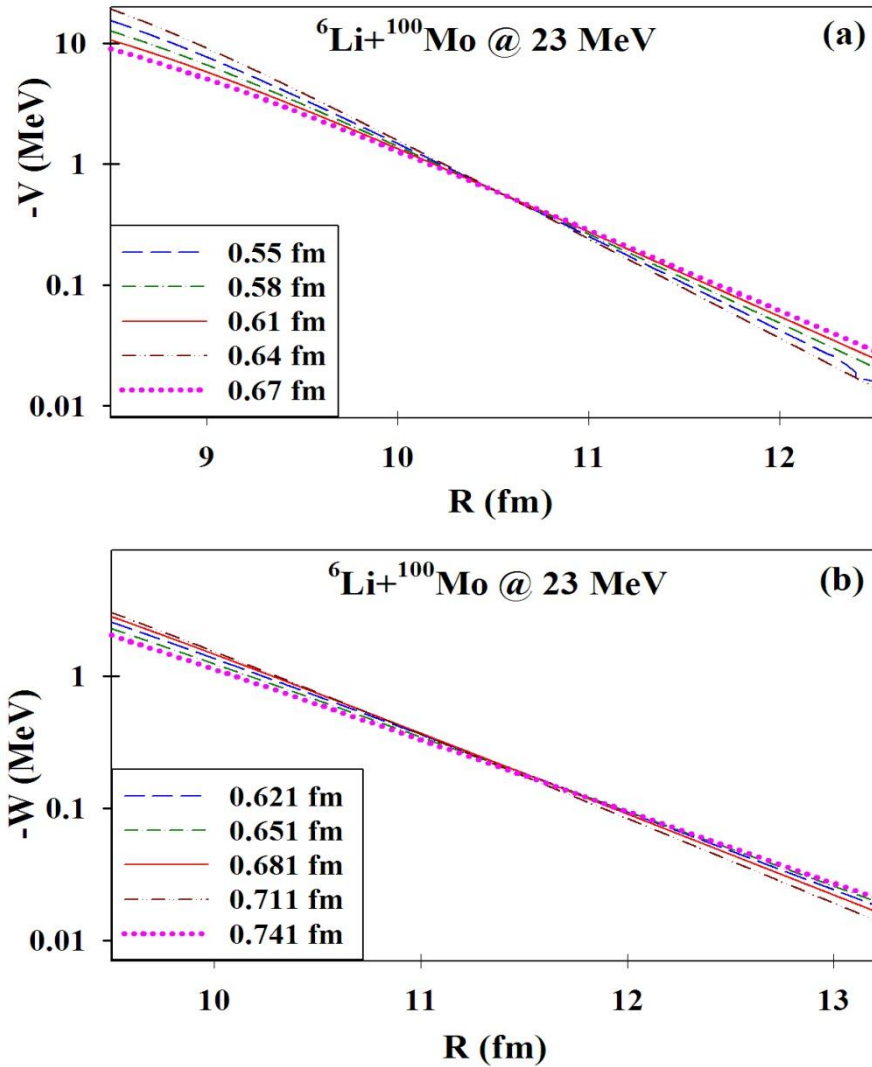


Figure 6.3: The sensitivity radius deduced from optical model analysis for the real and imaginary parts for the system ${}^6\text{Li}+{}^{100}\text{Mo}$ system at energy 23 MeV.

6.3.2 Dispersion Calculation

Dispersion relation guides the bridging of the optical potential's real and imaginary portions [5]. The interdependence of real and imaginary components is established using dispersion relation [15] as follows:

$$V(r, E) = V_0(r, E) + \Delta V(r, E)$$

and

$$\Delta V(r, E) = \frac{P}{\pi} \int_0^\infty \frac{W(r, E')}{E' - E} dE' \quad (6.3)$$

$\Delta V(r, E)$ is an attractive polarization potential and depends on imaginary potential $W(r, E')$ (detailed over the topic are mentioned in chapter 2 (section 2.3)) whose shape is assumed to be clubbed of two /three segments and their associated real potential is generated through dispersion relation calculations. Figures 6.4 show the results of dispersion relation for ${}^6\text{Li}+{}^{100}\text{Mo}$ system. This can be noted that imaginary part rises before decreasing in the near barrier region and producing a corresponding dip in the real potential indicating BTA behavior around the Coulomb barrier for system ${}^6\text{Li}+{}^{100}\text{Mo}$ [14].

for ${}^6\text{Li}+{}^{100}\text{Mo}$ System

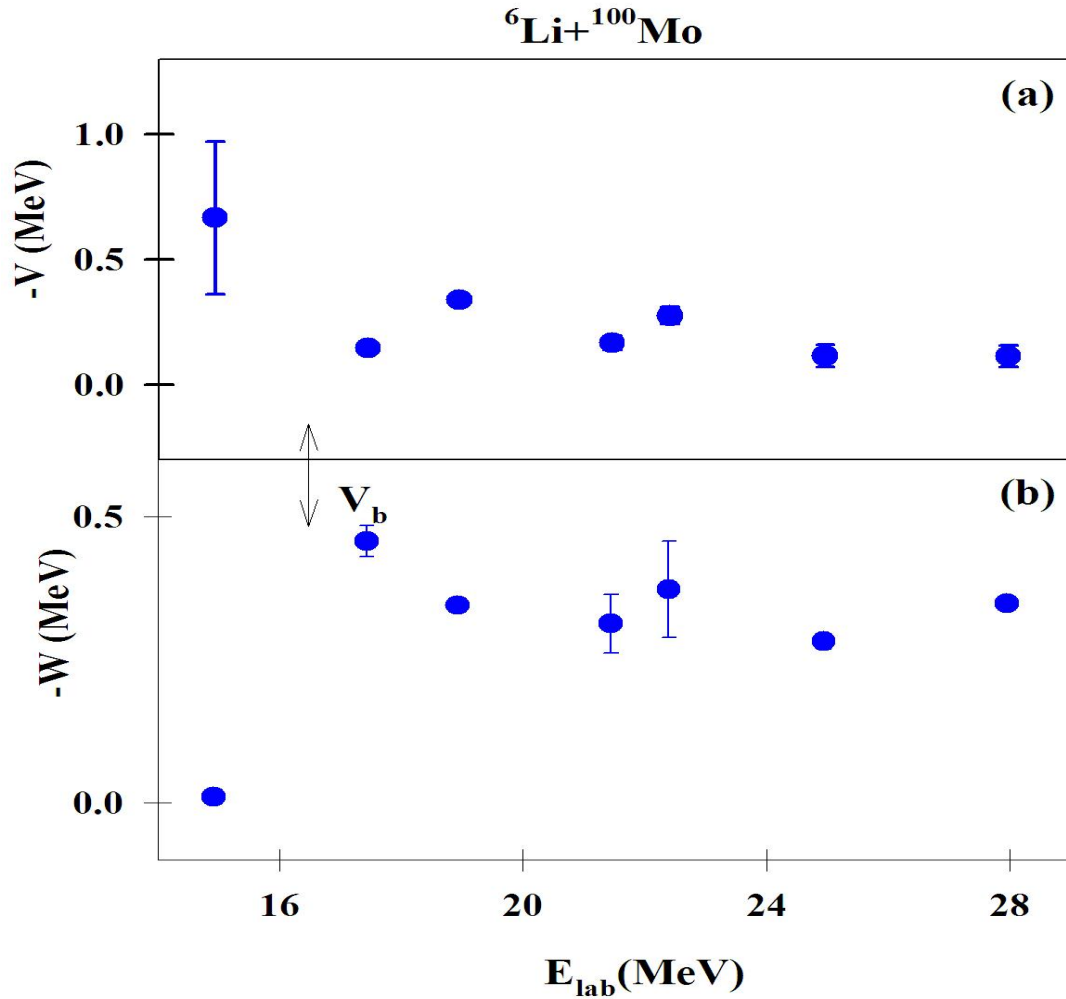


Figure 6.4: Real and imaginary potentials at sensitivity radius $R=10.97$ fm using optical model

WSP (blue solid circle).

6.4 Summary and Conclusions:

In this given work, we have done experiment for elastic scattering angular distribution for the systems ${}^6\text{Li}+{}^{100}\text{Mo}$ around the Coulomb barrier energies. The phenomenological optical model analysis of measurements was accomplished using Woods-Saxon potential. Calculations of the potential parameters and their energy dependence are done at sensitivity radii. The parameters demonstrate an increase in imaginary potential prior to adjacent of reaction channels. This is an indication of breakup threshold anomaly near by the Coulomb barrier for the middle mass region ${}^6\text{Li}+{}^{100}\text{Mo}$ system.

References

- [1] L. F. Canto, P. R. S. Gomes, R. Donangelo, and M. S. Hussein, Phys. Rep. 424, 1 (2006).
- [2] L. F. Canto, P. R. S. Gomes, R. Donangelo, J. Lubian, and M. Hussein, Phys. Rep. 596, 1 (2015).
- [3] J. J. Kolata, V. Guimares, and E. F. Aguilera, Eur. Phys. J. A 52, 123 (2016).
- [4] J. Lei and A. M. Moro, Phys. Rev. C 95, 044605 (2017).
- [5] G. R. Satchler, Phys. Rep. 199, 147 (1991).
- [6] J. Lei, A.M. Moro, Phys. Rev. Lett. 122, 042503 (2019).
- [7] K.J. Cook, E.C. Simpson, L.T. Bezzina, M. Dasgupta, D.J. Hinde, K. Banerjee, A.C. Berriman, C. Sengupta, Phys. Rev. Lett. 122, 102501 (2019).

Chapter 6: *Study of Breakup Effect of Weakly Bound Projectile around Coulomb Barrier Energies for ${}^6\text{Li}+{}^{100}\text{Mo}$ System*

- [8] C. Joshi, N. L. Singh, H. Kumawat, R. K. Singh et al., Proceedings of the DAE Symp. on Nucl. Phys. 66 (2022).
- [9] C. Joshi et al., DAE Symp. On Nucl.Phys. 63 (2018).
- [10] <http://www.iuac.res.in/elab/das/ppdas/Tutorials/fuman.html> (2020)
- [11] A. Chatterjee, LAMPS: Linux Advanced Multiparameter System (2008), <http://www.tifr.res.in/~pell/lamps.html>
- [12] A. Winther, Nucl. Phys. A 572, 191 (1994)
- [13] I. J. Thompson, FRESCO:version FRES 3.1 (2019), <http://www.fresco.org.uk/source/fres-v31.html>
- [14] C. Joshi, H. Kumawat, R. K. Singh, N. L. Singh, D. Patel, B. K. Nayak, J. Acharya, A. Parihari, K. Rani, S. D. Sharma, et al., Eur.Phys.J. A 57, 40 (2022).
- [15] M.S. Hussein, P.R.S. Gomes, J. Lubian, L.C. Chamon, Phys. Rev. C 73, 044610 (2006).

Chapter 6: *Study of Breakup Effect of Weakly Bound Projectile around Coulomb Barrier Energies*

for ${}^6\text{Li}+{}^{100}\text{Mo}$ System